Simulations of decohesion and slip of the $\Sigma_3\langle 111\rangle$ grain boundary in tungsten with non-empirically derived interatomic potentials: the influence of boron interstitials

2001 J. Phys.: Condens. Matter 13 6719

(http://iopscience.iop.org/0953-8984/13/31/311)

INSTITUTE OF PHYSICS PUBLISHING JOURNAL OF PHYSICS: CONDENSED MATTER

J. Phys.: Condens. Matter **13** (2001) 6719–6740 PII: S0953-8984(01)20506-2

Simulations of decohesion and slip of the $\Sigma_3\langle 111\rangle$ grain boundary in tungsten with non-empirically derived interatomic potentials: the influence of boron interstitials

Simon Dorfman[1], Vlad Liubich[2], David Fuks[2] and Kleber C Mundim[3]

[1] Department of Physics, Technion—Israel Institute of Technology, 32000 Haifa, Israel
[2] Department of Materials Engineering, Ben-Gurion University of the Negev, POB 653, Beer-Sheva, Israel
[3] Instituto de Quimica, Universidade de Brasilia, Caixa Postal 4478, 70919-970 Brasilia, Brazil

Received 5 January 2001, in final form 29 May 2001
Published 19 July 2001
Online at stacks.iop.org/JPhysCM/13/6719

Abstract

Monte Carlo atomistic simulations of the properties of $\Sigma_3\langle 111\rangle$ grain boundaries in W are carried out. We demonstrate the influence of boron additive on the resistance of the grain boundary with respect to different shifts. The interatomic potentials used in these simulations are obtained from *ab initio* total-energy calculations. These calculations are performed in the framework of density functional theory in the coherent potential approximation. A recursion procedure for extracting A–B-type interatomic potentials is suggested.

(Some figures in this article are in colour only in the electronic version)

1. Introduction

Grain boundaries (GBs) sliding in polycrystalline material play a dominant role in plastic behaviour at high temperatures. The contribution of GB sliding is estimated to be more than 60% in the case of micrograin superplastic deformation [1, 2], which is a totally inhomogeneous part of deformation, localizes in a limited zone near the GB, and strongly depends on the crystallographic structure of the GB. The cohesive energy of the GB is an additional physical quantity which characterizes the ductility of real metallic materials. The reduced cohesion of GBs is stated to be one of the major factors limiting ductility and, thus, the fabrication and reliability of high-strength metallic materials [3, 4]. Intergranular embrittlement in metals is usually caused by impurities segregating to the GBs. Impurities present in bulk concentrations of a thousand parts per million (ppm) may lead to drastic decreases of the ductility, fracture strength, etc. This poses significant processing and application problems and gave rise to the necessity to estimate energy values that may shed some light on the tendencies in material strengthening. In a series of papers [5, 6] a thermodynamic theory of embrittlement of interfaces

by solute segregation was developed. In this theory the important role is played by the quantity $2\gamma_{int}$, the Griffith ideal work of interfacial separation, which controls and determines the resistance of an interface to brittle fracture. It also depends on the crystallographic structure of the interface, on its detailed geometry, and on the type of the impurities that are segregated on the interface.

Because of the experimental difficulties of measuring the energy characteristics in the micrograin superplastic deformation, a lot of effort has been put into simulating GBs in metals. In [7] a first-principles simulation of GB sliding in Ge was reported. It was based on total-energy calculations with local pseudopotentials for the Ge ion cores. The sliding process has been simulated quasistatically. Prediction and observation of the structural reconstruction in pure Cu at the Σ_3 GB was discussed in [8], where a simple central-force N-body interatomic potential (IP) of the Finnis–Sinclair type [9, 10] was used. This IP was fitted to reproduce the equilibrium density, elastic modulus, and cohesive energy of Cu. Molecular dynamics and simulated annealing were used to study the asymmetrical Σ_3 tilt GB with a $\langle 211 \rangle$ rotation axis in Cu. The results of the predictions correspond well with the HRTEM image. In [11] it was shown that inclusion of the second and fourth moments of the electron spectra is sufficient to attain a satisfactory agreement with *ab initio* calculations of structural energy differences, broken-bond energies, and the energetics of the surface reconstruction.

Recent progress in developing highly efficient *ab initio* calculations has also made possible a systematic study of the role of impurities in intergranular cohesion on the electron–atom level [12]. The atomic configurations and energetics of As impurities in Si GBs were studied in [13] by combination of image intensity analysis and first-principles calculations with norm-conserving pseudopotentials. Such calculations, while being very helpful for elucidating the physics underlying cohesion/decohesion processes, do not allow one to quantify the ductilizing/embrittling capacity of impurities.

First-principles calculations are still too costly (due to the necessity of performing enormously time-consuming atomic relaxations, especially in the supercells with the GBs); therefore atomistic simulations may be quite helpful. In [14] the modified embedded-atom method (EAM) was applied in calculations of the energy characteristics of the $\Sigma_3\langle 111 \rangle$ GB in tungsten with different impurities located in the GB plane. Boron is of special interest in this regard, because in a lot of metals and alloys small boron additions modify their ambient-temperature properties (see, for example, reference [15]). Atomistic calculations were used to study the influence of alloying on the intergranular cohesion in W [16, 17]. On the basis of these simulations it was found that the cohesion of a GB appears to be the controlling factor limiting the ductility of high-strength metallic alloys, and particularly those containing W. These results are important for understanding the fundamental physics of interatomic interaction at the GB.

The purpose of our work is to calculate the energy of decohesion and the value of the slip energy barrier for $\Sigma_3\langle 111 \rangle$ GBs in pure tungsten and tungsten with boron additives which occupy the interstitial position at the GB. We will present the results of direct calculations of the shift along the GB and decohesion of the GB. In our calculations, non-empirical interatomic potentials are used. These potentials are extracted from *ab initio* calculations by a recursion procedure [18]. This procedure with some modifications was used in [19, 20] to study the dislocations, disordered phases, and free energies of the unstable stacking faults in Si. The model describes very well the local bonding for bulk defects and liquid and amorphous phases. In our simulations we extend the recursion procedure not only to obtain the interatomic potentials of pure elements but also to concentrate effort on finding a method for extracting the interactions of host A atoms with the impurity B. This problem is important if we are planning to study the influence of additives on the physical properties and relaxations in dilute solid solutions. We discuss the method of calculation of interatomic A–A and A–B potentials. In

section 2 of our paper we show the link of the excess mixing energy in substitutional solid solutions with the interatomic potentials and in section 3 we discuss a scheme for extracting them from the coherent potential approximation (CPA) calculations. Section 4 is devoted to the presentation of the formalism used to obtain three-body interatomic A–B potentials. The potentials obtained are used in section 5 to study the behaviour of the GB in tungsten with the boron atom placed in the trigonal prism environment of tungsten atoms. The relaxations of the atoms at the GB are simulated for shifts in the directions parallel and normal to the GB plane. In section 6 we discuss the results of our simulations for W–B solid solutions, and the results of simulations of GB elastic properties, and compare the formulated approach with the EAM formalism.

2. Mixing energy and interatomic potentials

The first step in developing AB interatomic potentials for solid solutions within the recursion procedure is based on data from non-empirical calculations of the cohesive energy. Assuming this energy to be known, we turn to the presentation of the cohesive energy in a substitutional solid solution in terms of pairwise interactions:

$$E = \frac{1}{2}\sum_{\substack{\vec{r},\vec{r}'\\ \vec{r}\neq\vec{r}'}} [V_{\mathrm{AA}}(\vec{r},\vec{r}')C_{\mathrm{A}}(\vec{r})C_{\mathrm{A}}(\vec{r}') + V_{\mathrm{BB}}(\vec{r},\vec{r}')C_{\mathrm{B}}(\vec{r})C_{\mathrm{B}}(\vec{r}') + 2V_{\mathrm{AB}}(\vec{r},\vec{r}')C_{\mathrm{A}}(\vec{r})C_{\mathrm{B}}(\vec{r}')] \tag{1}$$

where $V_{\mathrm{AA}}(\vec{r},\vec{r}')$, $V_{\mathrm{BB}}(\vec{r},\vec{r}')$, and $V_{\mathrm{AB}}(\vec{r},\vec{r}')$ are the pairwise interatomic potentials between atoms A, atoms B, and between A and B, respectively. The summation is performed over the vectors $\vec{r}$ and $\vec{r}'$; these are the lattice sites of the Ising lattice. The values $C_{\mathrm{A}}(\vec{r})$ and $C_{\mathrm{B}}(\vec{r}')$ are defined by the following relations:

$$C_{\mathrm{A}}(\vec{r}) = \begin{cases} 1 & \text{if the site } \vec{r} \text{ is occupied by the atom A} \\ 0 & \text{otherwise.} \end{cases}$$

$$C_{\mathrm{B}}(\vec{r}) = \begin{cases} 1 & \text{if the site } \vec{r} \text{ is occupied by the atom B} \\ 0 & \text{otherwise.} \end{cases}$$

Moreover, the condition

$$C_{\mathrm{A}}(\vec{r}) + C_{\mathrm{B}}(\vec{r}) = 1 \tag{2}$$

is satisfied which means that each site of the lattice is occupied by an atom A or an atom B. Substituting $C_{\mathrm{B}}(\vec{r})$ from equation (2) into equation (1) we obtain

$$E = \frac{1}{2}\sum_{\substack{\vec{r},\vec{r}'\\ \vec{r}\neq\vec{r}'}} \tilde{V}(\vec{r},\vec{r}')C_{\mathrm{A}}(\vec{r})C_{\mathrm{A}}(\vec{r}') + \frac{1}{2}\sum_{\vec{r}}[1-2C_{\mathrm{A}}(\vec{r})]\sum_{\vec{r}'} V_{\mathrm{BB}}(\vec{r},\vec{r}') + \sum_{\vec{r}} C_{\mathrm{A}}(\vec{r})\sum_{\vec{r}'} V_{\mathrm{AB}}(\vec{r},\vec{r}'). \tag{3}$$

Here

$$\tilde{V}(\vec{r},\vec{r}') = V_{\mathrm{AA}}(\vec{r},\vec{r}') + V_{\mathrm{BB}}(\vec{r},\vec{r}') - 2V_{\mathrm{AB}}(\vec{r},\vec{r}') \tag{4}$$

is the mixing potential. Taking it into account that

$$V_{\mathrm{BB}}(0) = \sum_{\vec{r},\vec{r}'} V_{\mathrm{BB}}(\vec{r},\vec{r}')$$

$$V_{\mathrm{AB}}(0) = \sum_{\vec{r},\vec{r}'} V_{\mathrm{AB}}(\vec{r},\vec{r}')$$

and

$$\sum_{\vec{r}} C_{\mathrm{A}}(\vec{r}) = N_{\mathrm{A}} \tag{5}$$

where N_{A} is the total number of atoms A, equation (3) takes the form

$$E = \frac{1}{2}\sum_{\substack{\vec{r},\vec{r}' \\ \vec{r}\neq\vec{r}'}} \tilde{V}(\vec{r},\vec{r}')C_{\mathrm{A}}(\vec{r})C_{\mathrm{A}}(\vec{r}') + \frac{1}{2}[N - 2N_{\mathrm{A}}]V_{\mathrm{BB}}(0) + N_{\mathrm{A}}V_{\mathrm{AB}}(0). \tag{6}$$

The energy per atom with $c_{\mathrm{A}} = N_{\mathrm{A}}/N$ is

$$E = \frac{1}{2N}\sum_{\substack{\vec{r},\vec{r}' \\ \vec{r}\neq\vec{r}'}} \tilde{V}(\vec{r},\vec{r}')C_{\mathrm{A}}(\vec{r})C_{\mathrm{A}}(\vec{r}') + \frac{1}{2}[1 - 2c_{\mathrm{A}}]V_{\mathrm{BB}}(0) + c_{\mathrm{A}}V_{\mathrm{AB}}(0). \tag{7}$$

The distribution of atoms A in such a binary alloy may be described by one occupation probability function $n(\vec{r})$, which is the probability of finding an atom A at the site $\vec{r}$ of the crystal lattice:

$$n(\vec{r}) = \langle C_{\mathrm{A}}(\vec{r})\rangle \tag{8}$$

where the averaging is done over the Gibbs canonical ensemble. Performing such averaging, it is possible to represent the energy per atom in the form

$$E = \frac{1}{2N}\sum_{\substack{\vec{r},\vec{r}' \\ \vec{r}\neq\vec{r}'}} \tilde{V}(\vec{r},\vec{r}')n(\vec{r})n(\vec{r}') + \frac{1}{2}[1 - 2c_{\mathrm{A}}]V_{\mathrm{BB}}(0) + c_{\mathrm{A}}V_{\mathrm{AB}}(0). \tag{9}$$

This approach was used in reference [21] to describe the ordering effects in a binary substitutional solid solution. Let us consider the case where all positions of the crystal lattice sites are described by one Bravais lattice. Following the works of Khachaturyan (see reference [21] and references therein), the function $n(\vec{r})$, which determines the distribution of solute atoms in an ordering phase, can be expanded in a Fourier series. It can be represented as a superposition of concentration waves (CWs):

$$n(\vec{r}) = c_{\mathrm{A}} + \frac{1}{2}\sum_{j}[Q(\vec{k}_j)\mathrm{e}^{\mathrm{i}\vec{k}_j\cdot\vec{r}} + Q^*(\vec{k}_j)\mathrm{e}^{-\mathrm{i}\vec{k}_j\cdot\vec{r}}] \tag{10}$$

where $\mathrm{e}^{\mathrm{i}\vec{k}_j\cdot\vec{r}}$ is a static CW, $\vec{k}_j$ is a non-zero wave vector defined in the first Brillouin zone of the disordered A–B alloy, the index j denotes the wave vectors in the Brillouin zone, and $Q(\vec{k}_j)$ is a CW amplitude. As shown in reference [21], all $Q(\vec{k}_j)$ are linear functions of the long-range-order parameters of the superlattices that may be formed on the basis of the Ising lattice of the disordered solid solution. The disappearance of the ordering state immediately leads to the statement that all $Q(\vec{k}_j)$ are equal to zero [22]. Thus equation (9) may be rewritten in the form

$$E(c) = \frac{1}{2}\tilde{V}(0)c_A^2 + \frac{1}{2}[1 - 2c_{\mathrm{A}}]V_{\mathrm{BB}}(0) + c_{\mathrm{A}}V_{\mathrm{AB}}(0) \tag{11}$$

where

$$\tilde{V}(0) = \sum_{\vec{r},\vec{r}'}[V_{\mathrm{AA}}(\vec{r},\vec{r}') + V_{\mathrm{BB}}(\vec{r},\vec{r}') - 2V_{\mathrm{AB}}(\vec{r},\vec{r}')]. \tag{12}$$

Equation (11) may be presented in the form

$$E(c_{\mathrm{A}}) = E(0) + c_{\mathrm{A}}E_{\mathrm{A}}^{(0)} + c_{\mathrm{A}}^2E_{\mathrm{A}}^{(1)} + \cdots \tag{13}$$

with $E_{\mathrm{A}}^{(1)} = \tilde{V}(0)/2$. To clarify the meaning of this coefficient, we may use the model of regular solid solutions (RSS) for alloys (see, for example, reference [23]):

$$E(c_{\mathrm{A}}) = c_{\mathrm{A}}E'_{\mathrm{A}} + (1 - c_{\mathrm{A}})E'_{\mathrm{A}} + Uc_{\mathrm{A}}(1 - c_{\mathrm{A}}) \tag{14a}$$

where E'_{A} and E'_{B} are the cohesive energies of the components A and B respectively, and the last term represents the mixing energy, ΔE, of such an alloy. It is important to note that in equation (14*a*), E'_{A} and E'_{B} are taken for the same crystalline lattice as the alloy. Here they are calculated at the equilibrium lattice parameter for the lattice under consideration. In other words, if, for example, the alloy exists in bcc structure, then E'_{A} and E'_{B} have to be calculated in the bcc lattice (even if they both or one of them actually does not exist in this lattice). Their values corresponding to the equilibrium lattice parameter of the bcc structure for *pure* A and B components should be taken. Comparing the c_{A}^2-terms in equations (13) and (14) one immediately gets

$$E_{\mathrm{A}}^{(1)} = \frac{\tilde{V}(0)}{2} = -U. \tag{14b}$$

Taking into account that in the approximation of pairwise interactions the cohesive energies of constituents are

$$E_{\mathrm{A}} = \frac{1}{2}\sum_{\substack{i,j \\ i\neq j}} V_{\mathrm{AA}}(|\vec{r}_i - \vec{r}'_j|) \qquad E_{\mathrm{B}} = \frac{1}{2}\sum_{\substack{i,j \\ i\neq j}} V_{\mathrm{BB}}(|\vec{r}_i - \vec{r}'_j|)$$

it is now easy to obtain using equation (12) the following relation:

$$\delta E = 2 \times \frac{1}{2}\sum_{\substack{i,j \\ i\neq j}} V_{\mathrm{AB}}(|\vec{r}_i - \vec{r}'_j|) = U + E_{\mathrm{A}} + E_{\mathrm{B}}. \tag{15}$$

It is easy to see from equation (12) that E_{A} and E_{B} in equation (15) have to be computed for the lattice parameter of the *alloy* in the pairwise approximation and thus they *do not coincide* with the values E'_{A} and E'_{B}. The result presented by equation (15) is very important because it allows one to extract interatomic potentials for distinct atoms from *ab initio* calculations.

3. Non-empirical pairwise potentials from CPA calculations

Large-scale atomistic simulations are still useful for modelling a GB with impurities and especially in the study of GB resistance to deformation, which we are going to consider. In this modelling the structural energy differences are important and the long-range interaction potentials are necessary in order to describe accurately a wide range of local atomic environments.

To obtain interacting potentials an exact procedure for inverting the *ab initio* energy data will be used in our simulations. The inversion approach was first formulated in [24] for the pair potentials and generalized for many-body potentials in [18, 25]. We present only the results for pair potentials, although the procedure for obtaining many-body interactions for binary systems is also discussed.

The non-empirical calculations were done in the framework of the single-site coherent potential approximation (CPA). The most attractive feature of the CPA is that this scheme can be applied to direct calculations of the electronic structure of randomly or partially ordered alloys [26–28]. Recent applications of the CPA scheme show that this method reproduces quite accurately the lattice parameters, the bulk modules, and the enthalpies of formation (see, e.g., reference [28] and references therein). This accuracy corresponds to the accuracy of other local density functional methods for completely ordered phases.

The scheme of calculations that is used in our paper includes several steps:

(a) In this step we perform the CPA calculations, in the framework of the linear muffin-tin orbital method (LMTO), of the total energies, E_{tot}, for pure tungsten and boron in the bcc lattice for various lattice parameters, a. These data are used to construct the pressure–volume diagram (equation of state) at $T = 0$ for pure elements. In other words we solve the equation

$$(\partial E_{tot}/\partial \Omega)_S = -p \tag{16}$$

for the set of pressures. The requirement that both components have to be calculated in the same (bcc, in our case) lattice is dictated by the definition of the mixing energy where all the energies have to be given in the same crystalline structure as the alloy of interest [23]. Now we use the definition of the cohesive energy

$$E = -\int_{\infty}^{\Omega_0} p \, \mathrm{d}\Omega = -\int_{\Omega_0}^{\infty} p \, \mathrm{d}\Omega \tag{17}$$

where Ω_0 is the equilibrium volume per atom for the pressure $p = 0$. Varying Ω_0 in this integral is equivalent to the uniform expansion or compression of the crystal. Performing such calculations we obtain the dependence of the cohesive energy on the lattice parameter. We consider only atomic volumes smaller than 10.50 au^3 to avoid the difficulty in the LDA of accurately representing the energies of isolated atoms [29]. Smooth interpolation of the LDA data and extrapolation to infinite volume with an exponential tail are used.

(b) With the dependence of cohesive energy on the distance (in the case of pairwise interactions) obtained, this energy can be written as

$$E(r) = \sum_{p=1}^{\infty} n_p V(s_p r) \tag{18}$$

with atomic separation grouped into coordination shells p of radius $s_p r$, containing n_p atoms each. Uniform dilatation of the lattice is described by varying the parameter r with the structural quantities $\{s_p\}$ and $\{n_p\}$ fixed. The shells are numbered such that $s_1 < s_2 < s_3 < \cdots$, and the distances scaled such that $s_1 = 1$. The desired inversion formula for $V[E]$ may be obtained from equation (18) by rearranging the terms:

$$V(r) = \frac{1}{n_1}\left(E(r) - \sum_{p=2}^{\infty} n_p V(s_p r)\right). \tag{19}$$

Recursive substitution now generates the explicit formula

$$V(r) = \frac{1}{n_1}E(r) - \sum_{p=2}^{\infty} \frac{n_p}{n_1^2} E(s_p r) + \sum_{p,q}^{\infty} \frac{n_p n_q}{n_1^3} E(s_p s_q r) - \cdots. \tag{20}$$

In this way we obtain the *ab initio* effective pair potentials for both pure tungsten and boron.

(c) In this step we calculate, in the framework of the CPA formalism, the total energy of an extremely dilute random solid solution of boron impurity in a tungsten host. The atomic fraction of boron is taken equal to 1 at.%. The calculations are done for different lattice parameters. This allows us to obtain the volume dependence of the cohesive energy per atom for such a solid solution in the same manner as explained in item (a) above.

(d) Using equation (14) we calculate the dependence of the parameter U on the distance, which together with equation (15) gives also the dependence of δE on the lattice parameter.

(e) Keeping in mind the first part of equation (15), the effective interatomic potentials $V_{\mathrm{AB}}(r)$ are calculated with the recursion formula (20), where we substitute $\delta E(r)/2$ for $E(r)$.

4. Many-body interactions in alloys derived from the recursion procedure

In this section we discuss the formalism used to obtain three-body interatomic potentials for host atoms with impurities. Our presentation includes not only the recursion formalism for interatomic interactions of A–A–A and B–B–B types but also A–A–B and A–B–B interactions. To study the many-body interactions in binary alloys we apply the scheme that was formulated in [18] for pure solids. In [18] the simplest case of a many-body potential was considered with volume-independent pair terms and separable three-body terms. For pure solids, subtracting the pair terms from the *ab initio* calculated cohesive energy, $E(r)$, forms the many-body energy, $F(r)$:

$$F(r) = E(r) - E^{(pair)}(r) \tag{21}$$

where $E^{(pair)}(r)$ is the energy, which is presented as a sum over pairwise interactions. The function $F(r)$ is expressed as a sum over pairs of bonds:

$$F(r) = \sum_i \sum_{\substack{j\neq i\\ j>i}} \sum_{\substack{k\neq i,\\ k>j}} g(r_{ij})g(r_{jk})h(\vartheta_{ijk}) \tag{22}$$

with $\cos\vartheta_{ijk} = (\vec{r}_{ij}\cdot\vec{r}_{jk})/(r_{ij}r_{jk})$ and $r_{ij} = |\vec{r}_i - \vec{r}_j|$. This function is assumed to be positive ($F(r) \geqslant 0$), on the basis of references [18, 30, 31]. Also a particular form for the angular term $h(\vartheta)$ must be assumed to invert $F[g, h]$ to get the radial function $g[F, h]$. The procedure for getting $g(r)$ is the same as in the pair potential case: solve equation (22) for $g(r)$ to obtain the recursion. Grouping bonds into shells, s_p, as in section 3 and taking the positive root of the resulting quadratic equation, the desired expression may be presented in the form

$$g(r) = \frac{-\beta(r) + \sqrt{[\beta(r)]^2 + 4\alpha_{11}[F(r) - \gamma(r)]}}{2\alpha_{11}} \tag{23}$$

where

$$\alpha_{pq} = \sum_{r_{ij}\in s_p} \sum_{r_{jk}\in s_q} h(\vartheta_{ijk}) \tag{24}$$

$$\beta(r) = \sum_{p=2}^{\infty} \alpha_{1p} g(s_p r) \tag{25}$$

$$\gamma = \sum_{p=2}^{\infty} \sum_{q=p}^{\infty} \alpha_{pq} g(s_p r) g(s_q r). \tag{26}$$

In the α_{pp}-sums one must only take $k > j$ contributions into account, to avoid double counting. An explicit formula like that for the pair potentials can be obtained by substituting in the recursion procedure using equation (23). The details of the procedure may be found in [18].

From the definition of the function $F(r)$ given by equations (21) and (22) we may note that accounting for three-body interactions is equivalent to the representation of the energy in terms of effective interactions, $V^*(r_i, r_j)$, by means of

$$E(r) = \frac{1}{2} \sum_{\substack{i,j\\ i\neq j}} V^*(r_i, r_j)$$

where

$$V^*(r_i, r_j) = V(r_i, r_j) + \sum_{\substack{k,\\ k\neq i, k>j}} g(r_{ij})g(r_{jk})h(\vartheta_{ijk}). \tag{27}$$

Here the first term is the pairwise potential and the second one describes the triple interaction as the angle-dependent interaction of two bonds. These bonds are given by the vectors $\vec{r}_{ij}$ and $\vec{r}_{jk}$. The energy of a binary system may now be written in the same form as equation (1) but with $V^*(r_i, r_j)$ substituting for $V(r_i, r_j)$ (which represented the pairwise interactions in equation (1)):

$$E = \frac{1}{2}\sum_{\substack{i,j \\ i\neq j}}(V^*_{\mathrm{AA}}(|\vec{r}_i - \vec{r}_j|)C_{\mathrm{A}}(\vec{r}_i)C_{\mathrm{A}}(\vec{r}_j) + V^*_{\mathrm{BB}}(|\vec{r}_i - \vec{r}_j|)C_{\mathrm{B}}(\vec{r}_i)C_{\mathrm{B}}(\vec{r}_j) + V^*_{\mathrm{AB}}(|\vec{r}_i - \vec{r}_j|)C_{\mathrm{A}}(\vec{r}_i)C_{\mathrm{B}}(\vec{r}_j) + V^*_{BA}(|\vec{r}_i - \vec{r}_j|)C_{\mathrm{B}}(\vec{r}_i)C_{\mathrm{A}}(\vec{r}_j)) \tag{28}$$

where

$$V^*_{\mathrm{AA}}(|\vec{r}_i - \vec{r}_j|) = V_{\mathrm{AA}}(|\vec{r}_i - \vec{r}_j|) + \sum_{\substack{k, \\ k\neq i, k>j}} g_{\mathrm{AA}}(r_{ij})g_{\mathrm{AA}}(r_{jk})h(\vartheta_{ijk})C_{\mathrm{A}}(\vec{r}_k) \tag{29}$$

$$V^*_{\mathrm{AB}}(|\vec{r}_i - \vec{r}_j|) = V_{\mathrm{AB}}(|\vec{r}_i - \vec{r}_j|) + \sum_{\substack{k, \\ k\neq i, k>j}} \{g_{\mathrm{AB}}(r_{ij})g_{\mathrm{AB}}(r_{jk})h(\vartheta_{ijk})C_{\mathrm{A}}(\vec{r}_k) + g_{\mathrm{AB}}(r_{ij})g_{\mathrm{BB}}(r_{jk})h(\vartheta_{ijk})C_{\mathrm{B}}(\vec{r}_k)\}. \tag{30}$$

The expression for $V_{\mathrm{BB}}(|\vec{r}_i - \vec{r}_j|)$ may be obtained from (29) by making the substitution A $\rightarrow$ B, and the expression for $V_{BA}(|\vec{r}_i - \vec{r}_j|)$ may be obtained from (30) by making the substitutions A $\rightarrow$ B, B $\rightarrow$ A. In the definition of the effective potentials the 'environment' of the pair of atoms is accounted for. Thus, for example, for the effective potential V^*_{AB}, both the interactions of the pair A–B with the third atom A and those with the third atom B are included. The type of the third atom and its location, i.e. the probability of finding it at the point r_k (when the atom A is in the position r_i and B is at r_j) is regulated by the occupation number $C_{\mathrm{A}}(r_k)$ or $C_{\mathrm{B}}(r_k)$.

After making the substitution $C_{\mathrm{B}}(\vec{r}_\lambda) = 1 - C_{\mathrm{A}}(\vec{r}_\lambda)$ with $\lambda = i, j, k$ in equations (29) and (30), the equation for the energy takes the form (compare with equation (1))

$$\begin{aligned} E = \frac{1}{2}\sum_{\substack{i,j \\ i\neq j}}\Big\{ & V_{\mathrm{AA}}(|\vec{r}_i - \vec{r}_j|)C_{\mathrm{A}}(\vec{r}_i)C_{\mathrm{A}}(\vec{r}_j) + V_{\mathrm{BB}}(|\vec{r}_i - \vec{r}_j|)[1 - C_{\mathrm{A}}(\vec{r}_i)][1 - C_{\mathrm{A}}(\vec{r}_j)] \\ & + V_{\mathrm{AB}}(|\vec{r}_i - \vec{r}_j|)C_{\mathrm{A}}(\vec{r}_i)[1 - C_{\mathrm{A}}(\vec{r}_j)] + V_{BA}(|r_i - \vec{r}_j|)[1 - C_{\mathrm{A}}(\vec{r}_i)]C_{\mathrm{A}}(\vec{r}_j) \\ & + \sum_{\substack{k, \\ k\neq i, k>j}} \{g_{\mathrm{AA}}(r_{ij})g_{\mathrm{AA}}(r_{jk})h(\vartheta_{ijk})C_{\mathrm{A}}(\vec{r}_i)C_{\mathrm{A}}(\vec{r}_j)C_{\mathrm{A}}(\vec{r}_k) \\ & + g_{\mathrm{BB}}(r_{ij})g_{\mathrm{BB}}(r_{jk})h(\vartheta_{ijk})[1 - C_{\mathrm{A}}(\vec{r}_i)][1 - C(\vec{r}_j)][1 - C(\vec{r}_k)] \\ & + g_{\mathrm{AB}}(r_{ij})g_{\mathrm{AB}}(r_{jk})h(\vartheta_{ijk})C_{\mathrm{A}}(\vec{r}_i)[1 - C_{\mathrm{A}}(\vec{r}_j)]C_{\mathrm{A}}(\vec{r}_k) \\ & + g_{\mathrm{AB}}(r_{ij})g_{\mathrm{BB}}(r_{jk})h(\vartheta_{ijk})C_{\mathrm{A}}(\vec{r}_i)[1 - C_{\mathrm{A}}(\vec{r}_j)][1 - C_{\mathrm{A}}(\vec{r}_k)] \\ & + g_{\mathrm{AB}}(r_{ij})g_{\mathrm{AA}}(r_{jk})h(\vartheta_{ijk})[1 - C_{\mathrm{A}}(\vec{r}_i)]C_{\mathrm{A}}(\vec{r}_j)C_{\mathrm{A}}(\vec{r}_k) \\ & + g_{\mathrm{AB}}(r_{ij})g_{\mathrm{AB}}(r_{jk})h(\vartheta_{ijk})[1 - C_{\mathrm{A}}(\vec{r}_i)]C_{\mathrm{A}}(\vec{r}_j)[1 - C_{\mathrm{A}}(\vec{r}_k)]\}\Big\}. \end{aligned} \tag{31}$$

After multiplication of the square brackets, averaging over the Gibbs canonical ensemble as in section 2, and assuming a random solid solution, we obtain the equation for $\tilde{V}^*(0)$ which unlike $\tilde{V}(0)$ includes three-body interactions. The details of the technique used to calculate the averaged values $\langle C_{\mathrm{A}}(\vec{r}_i)C_{\mathrm{A}}(\vec{r}_j)C_{\mathrm{A}}(\vec{r}_k)\rangle$ may be found in reference [32].

Now for the quantity U which is defined as in equation (14*b*) but with $\tilde{V}^*(0)$ instead of $\tilde{V}(0)$, we get

$$U(c_A) = -\frac{1}{2}\Bigg\{\sum_{\substack{i,j\\ i\neq j}}\{[V_{AA}(|\vec{r}_i-\vec{r}_j|)+V_{BB}(|\vec{r}_i-\vec{r}_j|)-2V_{AB}(|\vec{r}_i-\vec{r}_j|)] + \sum_{\substack{k,\\ k\neq i,k>j}}\{g_{AA}(r_{ij})g_{AA}(r_{jk})h(\vartheta_{ijk})c_A + g_{BB}(r_{ij})g_{BB}(r_{jk})h(\vartheta_{ijk})[3-c_A] - g_{AB}(r_{ij})g_{AB}(r_{jk})h(\vartheta_{ijk}) + g_{AB}(r_{ij})g_{AA}(r_{jk})h(\vartheta_{ijk})[1-c_A] + g_{AB}(r_{ij})g_{BB}(r_{jk})h(\vartheta_{ijk})[c_A-2]\}\Bigg\}. \tag{32}$$

It is easy to see that U now includes pairwise interactions that do not contain the concentration directly and three-body interactions that manifestly contain the concentration.

Let us turn to defining the radial functions $g(r)$. For the case of interaction of atoms of the same type, it may be done as for pure elements (see equation (23)). The result obtained for $U(c_A)$ given by equation (32) allows one to construct the additional function $F_2[g_{AB}, h]$. This function depends on the radial function $g_{AB}(r)$ which defines the three-body interactions between distinct atoms and makes it possible to apply the recursion procedure. $F_2[g_{AB}, h]$ is given by the following equation:

$$F_2 = \sum_i \sum_{\substack{j\neq i,\\ j>i}} \sum_{\substack{k\neq i,\\ k>j}} \{g_{AB}(r_{ij})g_{AB}(r_{jk}) + g_{AB}(r_{ij})[g_{AA}(r_{jk})(c_A-1)+g_{BB}(r_{jk})(2-c_A)]\}h(\vartheta_{ijk}) \tag{33}$$

and is defined as

$$F_2 = U + E''_A + E''_B - 2E'_{AB} + F_1 \tag{34}$$

where

$$E''_A = \frac{1}{2}\sum_{\substack{i,j\\ i\neq j}} V_{AA}(|\vec{r}_i-\vec{r}_j|) + \sum_{\substack{i,j,k\\ j>i,k>j}} g_{AA}(r_{ij})g_{AA}(r_{jk})h(\vartheta_{ijk}) \tag{35}$$

$$E'_{AB} = \frac{1}{2}\sum_{\substack{i,j\\ i\neq j}} V_{AB}(|\vec{r}_i-\vec{r}_j|) \tag{36}$$

$$F_1 = \sum_i \sum_{\substack{j,\\ j>i}} \sum_{\substack{k,\\ k>j}} [g_{AA}(r_{ij})g_{AA}(r_{jk})(c_A-1)+g_{BB}(r_{ij})g_{BB}(r_{jk})(2-c_A)]h(\vartheta_{ijk}). \tag{37}$$

E''_B may be obtained from equation (35) by making the substitution B $\rightarrow$ A. To calculate the radial function $g_{AB}(r)$ for distinct atoms, we have to follow a scheme:

(1) calculate the pairwise interatomic potentials $V_{AA}(r)$, $V_{BB}(r)$, $V_{AB}(r)$ as explained in sections 3 and 4;
(2) calculate the radial functions $g_{AA}(r)$ and $g_{BB}(r)$ using equations (21)–(23);
(3) define the function $F_2(r)$ using equations (34)–(37);
(4) solve equation (33), quadratic with respect to $g_{AB}(r)$, which is analogous to the corresponding equation for atoms of the same type;
(5) use the recursion procedure to finally obtain $g_{AB}(r)$.

5. Results of simulations

5.1. Development of potentials

The total-energy calculations were performed in the scalar-relativistic approach for a number of different volumes per atom. All of the calculations were done in the framework of the LMTO method in the CPA. The convergence criterion for the total energy was 0.001 mRyd. Details of our calculations are reported in [33]. The dependencies of the cohesive energies on the distance obtained were used to calculate the effective potentials $V_{W-W}(r)$, $V_{B-B}(r)$, and $V_{W-B}(r)$ by means of the recursion formula, as was discussed in section 3. These potentials were obtained in numerical forms and they could be satisfactorily described by the Morse function

$$V(r) = De^{-2\lambda(r-r_0)} - 2De^{-\lambda(r-r_0)}. \tag{38}$$

We have plotted these potentials in figure 1. The values of the parameters in equation (38) are given in table 1. Convergence of the recursion formula was checked in the following way: we assumed the cohesive energies to be equal to zero at the distances corresponding to the third, fourth, etc coordination shells (the cut-off radius). We found that the averaged relative difference in potentials when changing the cut-off radius from the seventh to the eighth shell is less than 0.1%.

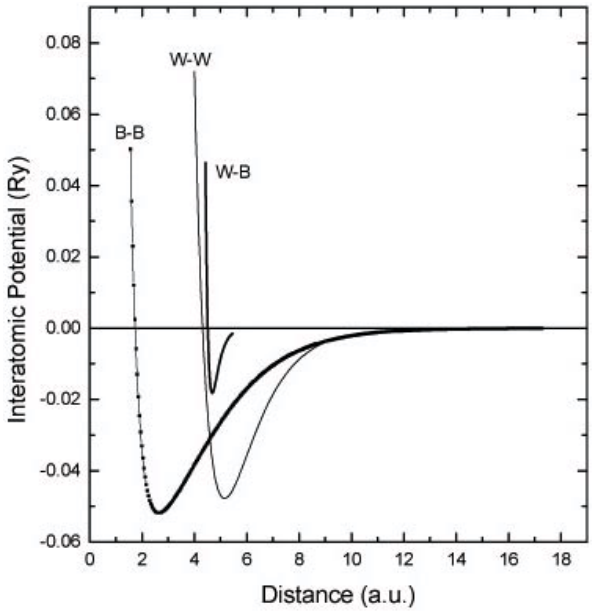

Figure 1. Interatomic potentials $V_{W-W}(r)$, $V_{B-B}(r)$, and $V_{W-B}(r)$ obtained by means of the recursion equation from the non-empirically calculated dependencies of cohesive energies on the distance.

To examine the quality of the potentials obtained and the validity of the procedure used, the Debye temperature for W was calculated. We explored the same methodology as in [34]. The value obtained, 410 K, is in excellent agreement with the measured one (392 K).

After that we checked the applicability of this potential to the properties where the relaxation effects are important and play a substantial role. To optimize the geometry, the Monte Carlo (MC) method was used in the generalized simulated-annealing approach (GSA)

Table 1. Parameters of Morse-type potentials.

D (Ryd)	λ (au^{-1})	r_0 (au)	Interacting atoms
0.04775	0.82330	5.15278	W–W
0.05177	0.57189	2.64138	B–B
0.01816	4.17256	4.67315	W–B

[35–37]. The GSA is based on the correlation between the minimization of a cost function (conformational energy) and the geometry randomly obtained through slow cooling. In this technique, an artificial temperature is introduced, and the system is gradually cooled in complete analogy with the well known annealing technique used in metallurgy when a molten metal reaches its crystalline state (the global minimum of the thermodynamic energy). In our case the temperature plays the role of an external noise.

The artificial temperature (or a set of temperatures) acts as a convenient stochastic source for eventual detraining from local minima. Near the end of the process the system is found within the attractive basin of the global minimum. The challenge is to cool the system as fast as possible and still guarantee that no irreversible trapping at any local minimum has occurred. More precisely, we search for the fastest annealing (which approaches quenching) that allows finishing the process within the global minimum with the probability equal to one.

The W–W potential (figure 1) was verified in atomistic simulations of a vacancy and di-vacancy in W. We used a large cluster with more than 5000 atoms. The vacancy was formed in the centre of the simulation volume. To decrease the computation time, the embedded-field method was used. In this method a cluster of a much smaller size with 89 atoms of W in the centre of the large cluster was chosen and the atoms inside this volume were allowed to relax. The inner cluster is situated in the field of the remaining part of the large cluster. Thus each atom inside the small cluster is relaxing in the constant field created by the outward part and in the field of the other relaxing atoms. This last field is time dependent during the calculation process and depends on the positions of other relaxing atoms.

Our simulations of the energy of the vacancy formation in W in the framework of MC GSA approach give $E_f^{(\mathrm{v})} = 4.23$ eV. This is in good agreement with experimental data and with the results of other calculations [38]. We calculated also the value of the diffusion barrier for the self-diffusion in W, simulating the movement of the atom from the position $(a/2)(111)$ to $(a/2)(000)$ where the vacancy was situated. In these calculations we relaxed the lattice at each step of the atom's movement along the diffusion path. The value of the energy barrier obtained, which is the migration energy for the self-diffusion in W, is equal to 1.67 eV (the experimental datum from [39, 40] is 1.63 eV).

In the next step of the calculations we formed two vacancies in the cluster. One of them was located at (000) while the second one occupied the position of its first, second, etc neighbour. Again, the geometry of the cluster was relaxed and the energy of the di-vacancy formation, $E_f^{(2\mathrm{v})}$, was calculated. The binding energy, $E_{bind}^{(2\mathrm{v})}$, of the di-vacancy in tungsten is defined as $E_{bind}^{(2\mathrm{v})} = E_f^{(2\mathrm{v})} - 2E_f^{(v)}$. The results of the calculations are given in table 2. As follows from these data, the binding energy for the di-vacancy in W is negative for the closest distance between mono-vacancies and becomes positive for all other distances considered. Such dependence proves the stability of short-range di-vacancy complexes in bcc W. Di-vacancy formation is known to be one of the possible explanations of the deviation from the Arrhenius law in the self-diffusion in bcc metals. The existence of the long-range interaction of vacancies in W is also clearly demonstrated by the data from table 2, but more distant configurations of di-vacancies are obtained as being unstable as compared with mono-vacancy formation.

Table 2. Energies of formation and binding energies of di-vacancies (in eV) that are formed as the first, second, etc neighbours in bcc W.

Neighbours	$E_f^{(2v)}$	$E_{bind}^{(2v)}$
1	8.140	−0.32
2	8.470	0.010
3	8.755	0.295
4	8.650	0.190
5	8.777	0.317
6	8.720	0.260
7	8.562	0.102

Unfortunately we have not succeeded in finding any reliable information for testing W–B and B–B potentials (figure 1). The reasons are obvious: B is typically in the amorphous state. A good test for the B–B IP should be a comparison of the formation energies aimed at studying the relative stability of different polymorphic modifications of B. As far as we know, experimental data on B amorphous structure are rare and not well established. In this case it would be a purely scientific exercise to compare these energies. The accuracy of determination of the relative stability of different B allotropic phases (including the amorphous one with the measured radial distribution function) does not allow comparison of theoretical data with experimentally obtained enthalpies of formation. The comparison of any experimental data on dilute solid solutions of B in W hosts with non-empirical calculations is even more complicated: typically these solutions have the same properties as the host. Theoretical simulations become highly attractive here.

5.2. Application to the grain boundary

The reported potentials were applied to simulate the relaxation of the $\Sigma_3\langle 111\rangle$ GB in tungsten. In figure 2 we show the structure of the part of the cluster that was used in these simulations. One boron atom was located in the trigonal prism interstitial position at the GB. For the chosen cluster this corresponds to a concentration of B at the GB equal approximately to 1 at.%. Periodic boundary conditions were used. Nine planes above and below the GB were allowed to relax. Thus, the distance between the GBs periodic in the Z-direction is 18 planes, which allows us to assume that GBs do not interact with each other. In figure 3 the GB is located at $Z = 0$, while the direction X is defined from the left to the right side in figure 3(b). The axis Z was directed normally to the plane of the GB with the positive direction to the upper part of the figure. The initial cluster consisted of 432 atoms for simulations in tungsten and one B atom was added then to simulate its influence on the properties of the GB. The cluster was relaxed using the GSA technique without and with the B atom. We performed several different simulations. In the first step the atoms in the initial cluster with the GB were relaxed. After that the lower part of the cluster was shifted along the X-direction. This shift was performed with the step 0.5 Å. At each step the system was relaxed to obtain the minimal total energy, which was calculated together with the energies of shifted but non-relaxed configurations. The number of configurations treated at each step was about 10^6. In figure 3 we show, as an example, the relaxed configurations of the cluster in the vicinity of the GB with non-shifted parts of the cluster and the same when they are shifted by 2.5 Å. The difference between the energies per atom for relaxed and non-relaxed configurations represents the averaged elastic energy. This value was calculated for each step of the shifting process. To display the result obtained, we calculated the change in the averaged energy per atom for relaxed and 'shifted' systems with

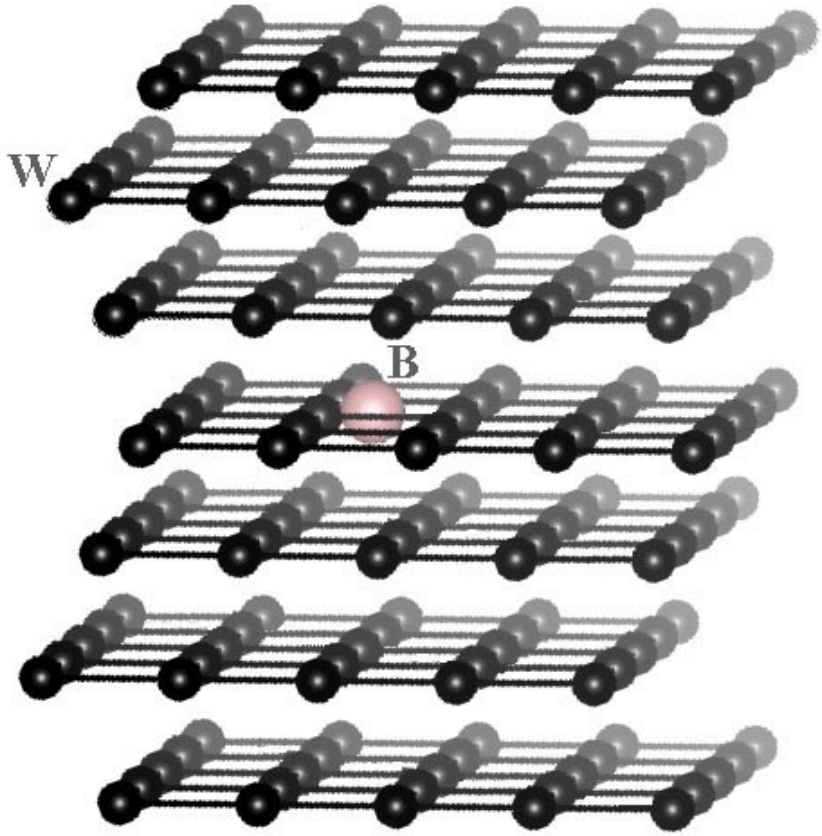

(a)

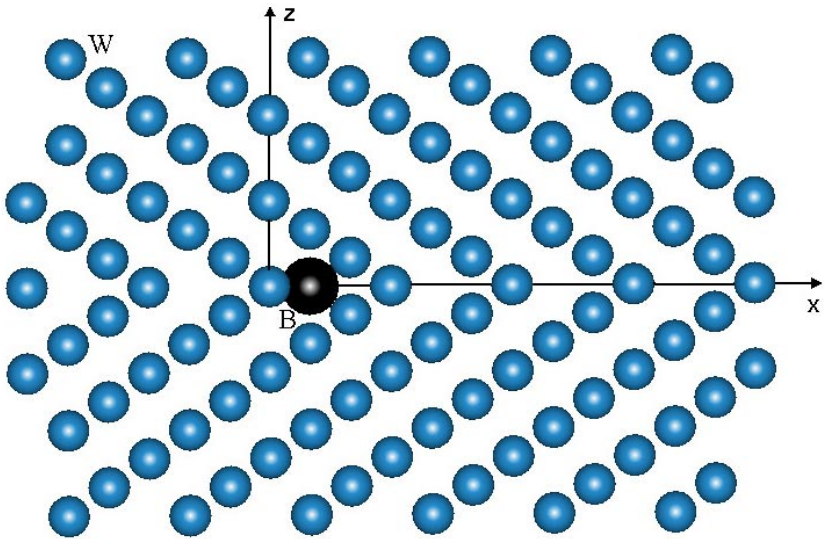

(b)

Figure 2. A part of the simulation cluster with the $\Sigma_3\langle 111\rangle$ grain boundary: (a) isometric view; (b) side view.

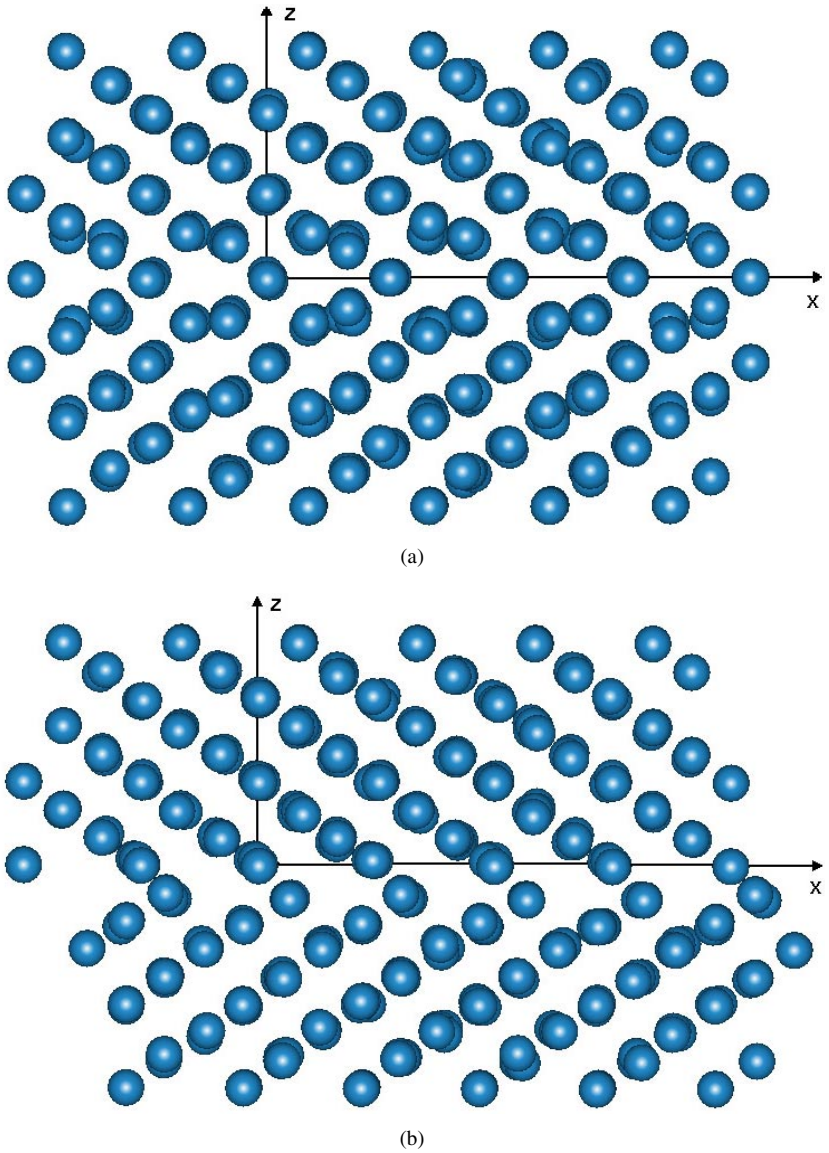

Figure 3. A side view of the relaxed $\Sigma_3\langle 111\rangle$ grain boundary: (a) the non-shifted cluster; (b) the lower part of the cluster is shifted by 2.5 Å.

respect to the same energy for the 'non-shifted' state of the system (see figure 4). The same procedure was repeated with the cluster containing the B atom at the grain boundary and a similar curve is also plotted in figure 4. It is easy to see that the presence of B on the $\Sigma_3\langle 111\rangle$ GB of tungsten increases the value of the energy barrier significantly. Thus boron prevents sliding along the GB and increases the resistance with respect to the shift in this direction.

The next series of computations were devoted to the simulation of the separation of two parts of the cluster in the Z-direction (decohesion). As in the previous case, the step in the shifting process was 0.5 Å, and in each step the system was allowed to relax. The corresponding change of the energy with respect to the energy of the non-shifted state of the system is given

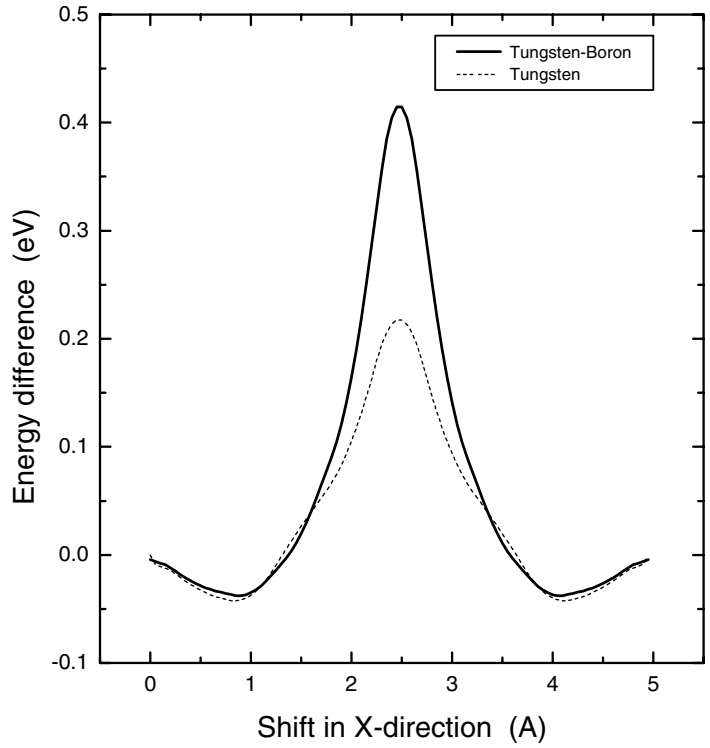

Figure 4. The profile of the energy barrier for the simulations of the $\Sigma_3\langle 111\rangle$ GB sliding along the X-direction. The dashed line is plotted for the calculations performed for the 'pure' W GB. The solid line corresponds to the simulations of the same sliding process for the case where B is placed at the GB as shown in figure 2.

in figure 5. In the simulations for the cluster with the B atom it was assumed to remain in the lower part of the separated system. It may be seen that for the separation process, a small amount of boron at the GB does not significantly influence the energy of the system and does not change the 'formation energy' of the GB. This conclusion does not apply to the case where the concentration of B at the GB is not small. The reason for this result is that the W–B potential that was obtained from *ab initio* calculations and the recursion procedure comes out short ranged as compared with the W–W interatomic potential. Thus, in the moving apart in the Z-direction, this potential does not significantly influence the elastic properties of the system. At the same time, it is worth noting that the effect would be much stronger if the number of B atoms at the GB were to be larger. This is not the case for the X-directional shift. Even a small amount of B at the GB drastically changes the resistance of the GB with respect to sliding. The reason is obvious: when, let us say, one of the W atoms moves away from B, the next atom along the grain boundary comes closer, thus approaching the 'active region' of repulsion in the W–B interaction.

To illustrate the distribution of the elastic field in the vicinity of the GB we present in table 3 the absolute values of the displacements of several atoms calculated with respect to the non-relaxed system. The same is given for the case where the lower part of the cluster is shifted by 2.5 Å in the X-direction. The location of the atoms is given in figure 6. The influence of a boron atom located at the GB on the displacements of the same tungsten atoms may be seen by comparison of these data with those presented on the right in this table. The

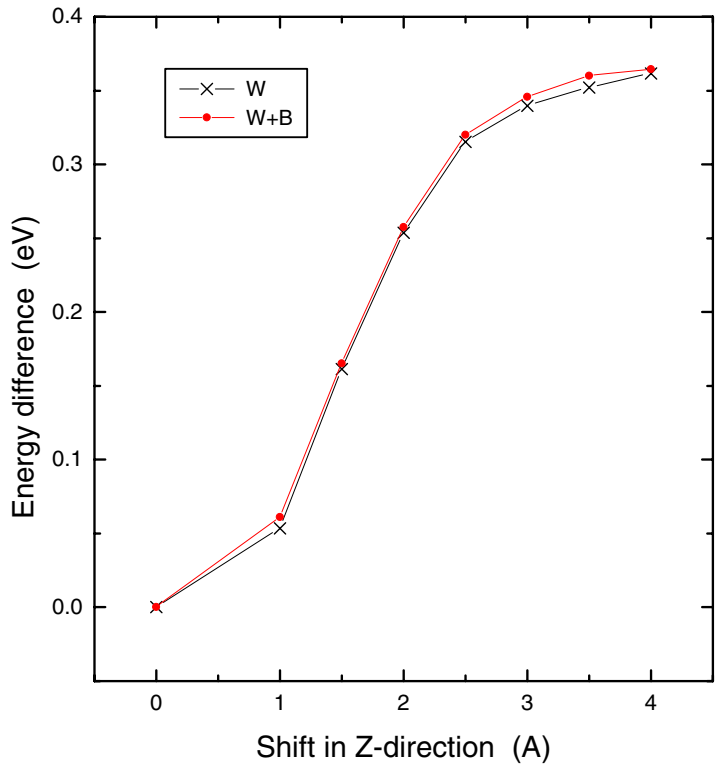

Figure 5. The change of the energy difference in the separation process in the direction normal to the $\Sigma_3\langle 111\rangle$ GB. The upper part of the simulation cluster is moved along the Z-direction. The curve with crosses displays the results for 'pure' GB, while the curve with black circles presents the results obtained with the B atom in the GB.

Table 3. Displacements of atoms (in Å) after relaxation in the vicinity of the tungsten GB with and without a B atom. The numbers of the atoms are the same as in figure 6. The data for the 'shifted' system correspond to a shift of 2.5 Å in the X-direction along the GB.

	W		W–B	
Number of atom	'Non-shifted'	'Shifted'	'Non-shifted'	'Shifted'
1	0.111	0.330	0.425	0.291
2	0.314	0.308	0.306	0.302
3	0.461	0.220	0.455	0.089
4	0.029	0.071	0.163	0.303
5	0.162	0.110	0.065	0.111
6	0.408	0.202	0.160	0.240
7	0.219	0.165	0.300	0.183

elastic field slowly decreases in the direction normal to the GB, as may be found by comparing the displacements of atoms N1 and N4, N2 and N5 etc. At the same time the relative change of the displacement in the case of the shifted GB is less than that for the non-shifted GB. A detailed comparative analysis of the fine atomic structure in the vicinity of the GB sheds some light on the behaviour of the system in the simulated process when the lower part of the cluster is shifted in the X-direction.

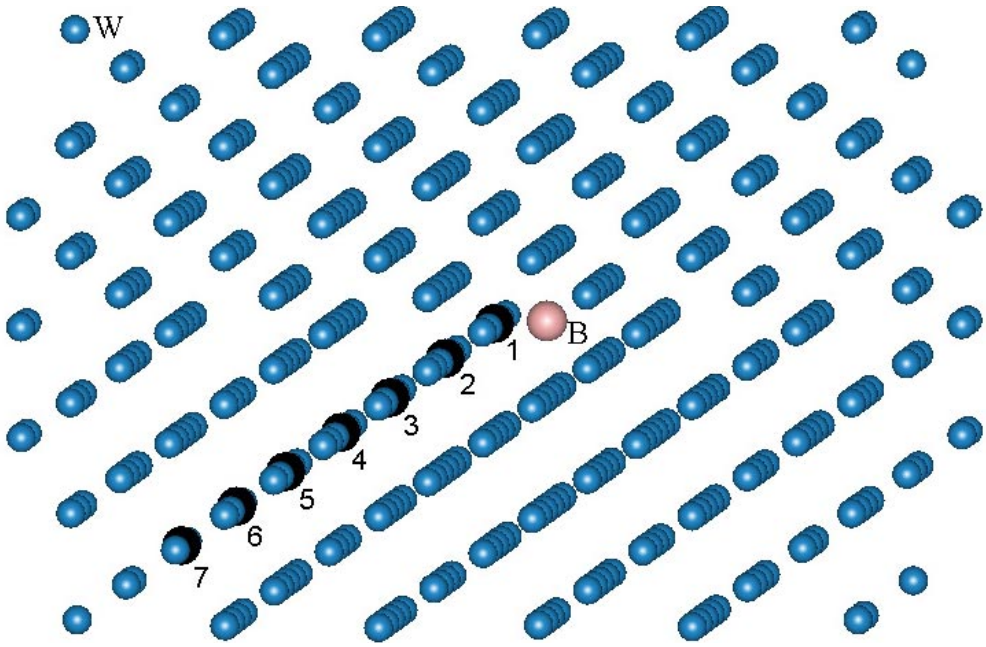

Figure 6. Positions of seven tungsten atoms in the vicinity of the $\Sigma_3\langle 111\rangle$ GB. The displacements of these atoms are given in table 3.

Let us consider the interactions of the atom N1 that is located at the GB with the rest of the atoms situated below the GB. A shift in the positive X-axis direction results in an increase in the average 'density' of atoms in the vicinity of atom N1. The effective distance from this atom to its nearest neighbours in the lower part of the cluster decreases and they 'feel' more strongly the repulsive part of the W–W interatomic potential. Thus, the energy of the system increases. At the same time, as illustrated by the data from table 3, the effective repulsion between atoms prevents relaxation of the lattice and the absolute values of the displacements for the 2.5 Å shift become smaller in comparison with those for the non-shifted GB. Further shift returns the system to the starting, 'non-shifted' situation because of the lattice periodicity in the X-direction. The presence of a boron atom at the GB makes the effect stronger. We locate this atom in the nearest neighbourhood of the atom N1 as shown in figure 6 and study the behaviour of the same atoms as in the case of the tungsten GB without boron. The repulsive W–B interaction increases the energy and prevents the displacements of the W atoms. The system now has a larger density of atoms in the vicinity of tungsten atom N1. Comparing the displacements of W atoms from table 3 for the 'non-shifted' case, we see that addition of boron effectively leads to a decrease in the absolute values of displacements. The system becomes more 'rigid'. The same happens when the lower part of the cluster shifts by 2.5 Å in the X-direction. Additional repulsion between B and W atoms increases the value of the energy barrier in the shifting process, thus improving the resistance of the system with respect to the X-directional shift.

To compute the tensile shift energy, γ_{tens}, associated with the shift in the X-direction along the $\Sigma_3\langle 111\rangle$ GB, we define it as the excess energy per unit surface area of the GB for the 'shifted' relaxed system relative to the one for the 'non-shifted' relaxed system. In the same manner we define the energy of decohesion of the GB, γ_{decoh}, as the difference between the energy per unit surface area of the GB for the relaxed system 'shifted' in the Z-direction relative

to the one for the 'non-shifted' relaxed system. As illustrated by figure 5, at distances between 3.5 Å and 4.0 Å the energy difference per atom in the separation process does not exceed 3%. The calculations show that this value changes insignificantly when the distance between the divided parts of the cluster changes from 6 Å to 6.5 Å. The value γ_{decoh} is calculated for the case where two parts of the simulation cluster are separated by the distance 6.5 Å. The influence of B on the energy characteristics γ_{tens} and γ_{decoh} of the GB in W is clearly seen from table 4. Both quantities increase as compared with those for the 'pure' GB. The relatively small increase of γ_{decoh} is due to the low boron concentration at the GB. Our estimations for the case where B occupies all interstitial sites in the trigonal prism position at the GB give γ_{decoh} equal to 0.613 eV Å^{-2}. Such a situation may occur if B atoms segregate to the GB. This leads to an increase of the amount of B at the GB and to a transfer of B from the bulk to the GB. These results on the influence of boron atoms on the mechanical properties of the GB correspond well with the results of molecular dynamics atomistic simulations reported in [14]. These simulations were performed for much higher concentrations of boron at the GB and with semi-empirical potentials. Unlike the authors of reference [14], we used in our simulations interatomic potentials extracted from *ab initio* calculations by an explicit inversion procedure. Experimental investigation of W alloyed with B revealed a significant drop in the ductile–brittle transition temperature [41–43]. We showed that even a small amount of B increases the fracture resistance of the $\Sigma_3\langle 111\rangle$ GB in W.

Table 4. Surface energy characteristics (in eV Å^{-2}) of the GB resistance with respect to a tensile shift and decohesion for the $\Sigma_3\langle 111\rangle$ GB in tungsten and for the GB with a boron atom.

Energies	$\Sigma_3\langle 111\rangle$ GB in tungsten	$\Sigma_3\langle 111\rangle$ GB in tungsten with boron interstitial
γ_{tens}	0.2420	0.4514
γ_{decoh}	0.3424	0.3457

Additional quantitative characterization of the effect of B on the sliding may be obtained from the dependences of the GB energy barriers on the relative displacement between the upper and lower parts of the simulation cluster, i.e., from the data on the fine profile of these barriers. The stress required to slide the equilibrium GB, σ_{slide}, is estimated as the maximal slope in the plots of GB energy versus relative displacement (see, for example, [44] and references therein):

$$\sigma_{slide} = \frac{\partial \gamma_{GB}}{\partial x_1} \tag{39}$$

where γ_{GB} is the GB energy. Our calculations show that this value for the 'pure' GB in W is about 29.5 GPa. The inclusion of B as the impurity in the GB increases this value and we get 48.6 GPa. We expect the σ_{slide}-values to be overestimated because only pairwise interactions were included in the simulations. Accounting for many-body interactions is known to decrease energy differences. So, the calculated values for stresses may become smaller, and the B effect may be less pronounced. However, the result obtained demonstrates the influence of B on the mechanical properties of the GB in W in the sliding process.

6. Discussion

We have presented in this work the results of a non-empirical study of the properties of the $\Sigma_3\langle 111\rangle$ GB in tungsten. A scheme for extracting the interatomic potentials of A–B type from *ab initio* calculations has been suggested. In contrast to the embedded-atom method

[45, 46], the formalism developed here makes it possible to account not only for A–A and B–B interactions, but also for A–B interactions in a binary system. This includes taking into account the three-body terms as well. Our approach allows A–A–B, A–B–B, and B–B–B interactions to be obtained. This is a distinguishing feature as compared with the Finnis–Sinclair method [47] that is usually called 'the N-body potential approach' and includes the effective atomic density-dependent term. The atomic density used in reference [47] actually represents an environment-dependent effective coordination number for the host system. Further modification of the method given in reference [17] includes addition of a term to the total energy. This term has the meaning of the energy of interaction between the impurity and host atoms. It is presented as a sum of 'environment-sensitive embedding' energies and is associated with the electron density at the site of the impurity atom due to the surrounding host atoms. At the same time, in these methods the interaction between impurities is not considered. This makes the application of these schemes to binary systems with non-small concentrations of impurities questionable. Our approach is free of this shortcoming.

It is worth comparing the scheme suggested in our simulations with the recursive potentials recently suggested in references [48–51]. The procedure that is used there to extract the interatomic potentials for host and impurity atoms is restricted: only the ordered phases in some stoichiometric compositions are considered. As follows from [50, 51], the potentials of A–B type are concentration dependent. This may be recognized by comparing the data obtained in [50, 51] for FeAl (B2) and Fe_3Al ($D0_3$), NiAl (B2) and NiAl (L_{12}), and for different Al–Li phases. The same result follows from *ab initio* calculations for the Fourier transforms of mixing potentials [52, 53]. Several additional comments should be made concerning the links of the formalism developed here with the phenomenological theory of solid solutions. The methodology that we suggest here allows accounting for the concentration dependence of A–B interatomic potentials in a direct way. The model of the RSS applied does not prevent one from obtaining this dependence. In fact, if U from equation (14) is a constant value independent of the concentration, then the potentials will also be concentration independent (actually there will still be some indirect dependence on concentration because of the changes of the lattice parameter of the alloy). At the same time, performing *ab initio* calculations for the mixing energy in binary disordered solid solutions at different concentrations, we may obtain the deviation from the RSS model. This means that U becomes a function of concentration and may be given as $U(c)$, which simply means that the mixing energy now has to be given in the form

$$\Delta E = U(c)_{\mathrm{A}} c_{\mathrm{A}}(1 - c_{\mathrm{A}}). \tag{40}$$

The functional form of $U(c_{\mathrm{A}})$ defines the deviation from the RSS model, and different types of this function determine subregular, subsubregular, etc solid solutions. The situation is well known from experiments. Such and more complicated models are often used in computer modelling of phase diagrams [23]. Our scheme for getting A–B interatomic potentials immediately generalizes to this case. For each concentration of interest, $c_{\mathrm{A}}^{(1)}$, the mixing energy has to be calculated as a function of the lattice parameter, a (or volume per atom). The quantity $U(c_{\mathrm{A}}^{(1)})$ as a function of a has to be calculated from equation (40) and the A–B interatomic potential for this concentration may be obtained with equation (15) using the recursion scheme. When concentration changes, the procedure has to be repeated. In our approach in the framework of the recursion procedure, we have to use the summation over the lattice vectors of the Ising lattice (that is, the lattice of the random solid solution). In the scheme presented, we do not need to concern ourselves with the possible superstructures that may appear if ordering occurs at some concentrations. This is justified by the fact that the effect of ordering on the interatomic potentials is very small and does not exceed several per cent

(see, for example, reference [54]). The concentration effects on the interatomic potentials are of much higher magnitude and we obtain, in principle, concentration-dependent potentials. Elsewhere, we will discuss the application of this scheme to the study of the ordering processes in alloys.

The formalism suggested in our paper for the development of the three-body interatomic potentials for binary solid solutions in some sense justifies the model of subregular solid solutions. It proves in a direct way that many-body (in our case, three-body) interactions in the alloy are responsible for the deviation from the regular solid-solution model. Concentrations of the elements enter the terms that are representing three-body interactions in our case. Together with the radial functions $g_{AA}(r)$, $g_{BB}(r)$, and $g_{AB}(r)$, this defines the deviation of U from the constant value. The statement formulated becomes more transparent on comparing the terms in the subregular solid-solution model with the theory derived above. In this model the mixing energy is given as

$$\Delta E = U(c_A)c_A(1 - c_A) = (L_0 + L_1c_A + L_2c_A^2 + \cdots)c_A(1 - c_A) \tag{41}$$

where $L_0, L_1, L_2, \ldots$ are constants. If the condition $L_1 = L_2 = \cdots = 0$ is satisfied, then equation (41) and $U = L_0$ give the RSS model. This situation was already discussed in section 3. It is clear that if $L_1 \neq 0$, then the corresponding term is linked to the three-body interactions, while L_0 includes pairwise interactions. If the four-body interactions are taken into account, then L_2 will become not equal to zero. Moreover, among four-body interactions there will be concentration-dependent terms that may be grouped with the three-body ones, i.e. included in L_1. Also, among the four-body interactions, concentration-independent terms will exist which may be formally included in L_0. This will renormalize L_1 which is responsible for the three-body interactions and L_0 which describes the pairwise interactions. We already have a similar result in our case: among the three-body interactions we see in U various terms that are concentration independent and may be formally included in L_0, thus renormalizing the pairwise interactions. Such a situation always occurs in the many-body theory, and detailed discussion on this subject may be found for example in reference [55].

Finally, the *ab initio* potentials obtained were applied in atomistic simulations. We demonstrated by means of direct calculations the influence of boron located in the tungsten GB on the resistance of the GB to shift in the plane of the GB and to GB formation. Our results demonstrate that B increases the energy of the GB decohesion and the resistance of GB with respect to tensile shift along the GB. The latter result is supported not only by the calculation of the relative change of the value of the energy barrier in the shifting process, but also by the fine profile of this barrier. Our conclusions coincide qualitatively with the findings of [14] and indirectly with experimental data [41–43].

Acknowledgments

This work was supported by the Israel Science Foundation founded by the Israel Academy of Sciences and Humanities (Grant No 380/97-11.7). We are greatly indebted to Dr A Ruban for support during our CPA calculations. We are grateful to Professor D E Ellis and Dr G Krasko for useful discussions. SD was supported by the 'KAMEA' programme.

References

[1] Mukerjee A K 1993 *Mater. Sci. Technol.* **6** 407
[2] Gifkins R C 1994 *Mater. Character.* **32** 59
[3] Guttmann M and McLean D 1979 *Interfacial Segregations* (Metals Park, OH: ASM) p 261

[4] Mescall J F and Rogers H 1987 *Proc. 34th Sagamore Army Materials Research Conf. on Innovations in Ultra-High Strength Steel Technology (Lake George, NY, 30 August–3 September)* ed G B Olson, M Azrin and E S Wright, pp 287–314
[5] Anderson P M, Wang J-S and Rice J R 1987 *Proc. 34th Sagamore Army Materials Research Conf. on Innovations in Ultra-High Strength Steel Technology (Lake George, NY, 30 August–3 September)* ed G B Olson, M Azrin and E S Wright, p 619
[6] Rice J R and Wang J-S 1989 *Mater. Sci. Eng.* A **107** 23
[7] Molteni C, Francis G P, Payne M C and Heine V 1996 *Phys. Rev. Lett.* **76** 1284
[8] Schmidt C, Ernst F, Finnis M W and Vitek V 1995 *Phys. Rev. Lett.* **75** 2160
[9] Ackland G J and Vitek V 1990 *Phys. Rev.* B **41** 10 324
[10] Foreman A J E, English C A and Phythian W J 1992 *Phil. Mag.* A **66** 655
[11] Carlsson A E 1991 *Phys. Rev.* B **44** 6590
[12] Krasko G L and Olson G B 1990 *Solid State Commun.* **76** 247
Krasko G L and Olson G B 1991 *Solid State Commun.* **79** 113
Krasko G L 1993 *Scr. Metall. Mater.* **28** 1543
Wu R, Freeman A J and Olson G B 1992 *J. Mater. Res.* **7** 2403
Wu R, Freeman A J and Olson G B 1993 *Phys. Rev.* B **47** 6885
Wu R, Freeman A J and Olson G B 1994 *Phys. Rev.* B **50** 75
Wu R, Freeman A J and Olson G B 1994 *Science* **265** 376
[13] Chisholm M F, Maiti A, Pennycook S J and Pantelides S T 1998 *Phys. Rev. Lett.* **81** 132
[14] Grujicic M, Zhao H and Krasko G L 1997 *Int. J. Refract. Met. Hard Mater.* **15** 341
[15] Baker I, Li X, Xiao H, Carleton R and George E P 1998 *Intermetallics* **6** 177
[16] Krasko G L 1997 *Mater. Sci. Eng.* A **234–236** 1071
[17] Krasko G L 1994 *Int. J. Refract. Hard Met.* **12** 251
[18] Bazant M Z and Kaxiras E 1996 *Phys. Rev. Lett.* **77** 4370
[19] Justo J F, Bazant M Z, Kaxiras E, Bulatov V V and Yip S 1998 *Phys. Rev.* B **58** 2539
[20] de Koning M, Antonelli A, Bazant M Z, Kaxiras E and Justo J F 1998 *Phys. Rev.* B **58** 12 555
[21] Khachaturyan A G 1983 *Theory of Structural Transformations in Solids* (New York: Wiley)
[22] Fuks D and Dorfman S 1994 *Phys. Rev.* B **50** 16 340
[23] Kaufman L and Bernstein H 1970 *Computer Calculations of Phase Diagrams* (New York: Academic)
[24] Carlsson A, Gelatt C and Ehrenreich H 1980 *Phil. Mag.* A **41** 241
[25] Bazant M Z and Kaxiras E 1996 *Materials Theory, Simulations and Parallel Algorithms (MRS Proc.)* ed E Kaxiras, J Joannopoulos, P Vashishta and R Kalia (Pittsburgh, PA: Materials Research Society) p 48
[26] Connolly J W D and Williams A R 1983 *Phys. Rev.* B **27** 5169
[27] Faulkner J S 1982 *Prog. Mater. Sci.* **27** 1
[28] Ruban A V, Abrikosov I A and Skriver H L 1995 *Phys. Rev.* B **51** 12 958
[29] Moll N, Bockstedte M, Fuchs M, Pehlke E and Scheffler M 1995 *Phys. Rev.* B **52** 2550
[30] Carlsson A E and Ashcroft N 1983 *Phys. Rev.* B **27** 2101
[31] Carlsson A E 1985 *Phys. Rev.* B **32** 4866
[32] Krivoglaz M A and Smirnov A 1964 *The Theory of Order–Disorder in Alloys* (London: Macdonald)
Badalyan D A and Khachaturyan A G 1970 *Sov. Phys.–Solid State* **12** 346
[33] Dorfman S 2000 *J. Phys.: Condens. Matter* **12** 4175
[34] Davidov G, Fuks D and Dorfman S 1995 *Phys. Rev.* B **51** 13 059
[35] Mundim K C and Tsallis C 1996 *Int. J. Quantum Chem.* **58** 373
[36] Moret M A, Pascutti P G, Bisch P M and Mundim K C 1998 *J. Comput. Chem.* **19** 647
Areas E P G, Pascutti P G, Schreier S, Mundim K C and Bisch P M 1995 *J. Phys. Chem.* **99** 14 882
[37] Ellis D E, Mundim K C, Fuks D, Dorfman S and Berner A 1999 *Phil. Mag.* B **79** 1615
[38] Xu Wei and Adams J B 1994 *Surf. Sci.* **301** 371
[39] Maier K, Peo M, Saile B, Shaefer H E and Seeger A 1979 *Phil. Mag.* A **40** 701
[40] Mundy J N, Rothman S J, Lam N Q, Hoff H A and Nowicki L J 1978 *Phys. Rev.* B **18** 6566
[41] Povarova K B *et al* 1990 *Izv. Acad. Nauk SSSR, Met.* **1** 76 (Engl. Transl. 1990 *Russ. Metall. Met.* **1** 74)
[42] Povarova K B *et al* 1987 *Izv. Acad. Nauk SSSR, Met.* **1** 134 (Engl. Transl. 1987 *Russ. Metall. Met.* **1** 129)
[43] Tolstobrov Yu O and Povarova K B 1987 *Fiz. Khim. Obrabot. Mater.* **21** 121 (in Russian)
[44] Kurtz R J, Hoagland R G and Hirth J P 1999 *Phil. Mag.* A **79** 665
[45] Daw M S and Baskes M I 1984 *Phys. Rev.* B **29** 6443
[46] Foiles S M, Baskes M I and Daw M S 1986 *Phys. Rev.* B **33** 7983
[47] Finnis M W and Sinclair J E 1984 *Phil. Mag.* A **50** 45
[48] Chen N X, Li M and Liu S J 1994 *Phys. Lett.* A **195** 135

[49] Ge X, Chen N X, Zhang W and Zhu F 1999 *J. Appl. Phys.* **85** 3488
[50] Zhang W, Xie Q and Ge X 1997 *J. Appl. Phys.* **82** 578
[51] Shaojun L, Suqing D and Benkun M 1998 *Phys. Rev.* B **58** 9705
[52] Liubich V, Dorfman S, Fuks D and Mehrer H 1999 *Mater. Trans. JIM* **40** 132
[53] Dorfman S, Fuks D and Liubich V 1998 *Int. J. Quantum Chem.* **70** 1067
[54] Fuks D L, Zhorovkov M F and Panin V E 1977 *Phys. Met. Metallogr.* **43** 139
[55] Mahan G D 1981 *Many-Particle Physics* (New York: Plenum)
de Fontaine D 1994 *Solid State Physics* vol 47, ed H Ehrenreich and D Turnbull (New York: Academic) p 33
Brovman E G and Kagan Yu M 1974 *Sov. Phys.–Usp.* **17** 125